Isotropically conducting tetraaryl osmium(IV), silane, and methane molecular wire junctions

Luana Zagami,[a] Cynthia Avedian,[a] Mukund Sharma,[a] Andrew Fraire,[a] Clarissa Olivar,[a] Daniel Hernangómez-Pérez,[b,*] and Michael S. Inkpen[a,*]

[a]*Department of Chemistry, University of Southern California, Los Angeles, CA 90089, USA*

[b]*CIC nanoGUNE BRTA, Tolosa Hiribidea, 76, 20018 Donostia-San Sebastián, Spain*

E-mail: d.hernangomez@nanogune.eu, inkpen@usc.edu

ABSTRACT

Structural motifs based on tetraphenylmethane have drawn substantial interest as components of molecular electronic circuits, self-assembled monolayers, and three-dimensional polymers. However, the broad utility of such motifs is limited, for example, by the broken conjugation though the central, sp^3-hybridized, carbon or silicon atom(s). To enrich their functionality, we reason the central atom could be exchanged for a transition metal to improve electronic coupling between the π-conjugated substituents and impart reversible redox properties. In evaluating this hypothesis, here we probe single-molecule junctions comprising oligoaryl wires with tetrahedral osmium(IV), silane, or methane centers. Surprisingly, we find that transport through junctions formed from the intact molecules in a non-polar, inert solvent appears largely independent of the central atom identity. In contrast, the conductance of junctions comprising an osmium(IV) wire can be modulated in an electrochemical environment by a factor of 47, to values 80× higher than for a silane analogue, by opening the bias window asymmetrically about the electrode Fermi level (E_F). These measurements also indicate that such compounds can undergo *in situ* reactions that result in junctions comprising their dissociated oligoaryl arms, linked by chemisorbed Au-C(sp^2) contacts. Our experimental results are supported by first principles calculations, which predict the osmium(IV) wires are substantially more conductive than the organic analogues due to their delocalized and well-coupled frontier orbitals with energies close to E_F. This work highlights the promising potential of transition metal tetraaryl complexes as isotropic building blocks for functional circuits and extended materials, while opening avenues for further studies to enhance the connection between experimental observations and theoretical calculations.

INTRODUCTION

In the development of molecular components that can function as electronic circuit elements such as wires or switches, most studies have focused on one-dimensional (1D) species functionalized with two linker groups to establish physical and electrical connections to nanoscale electrodes.[1] This emphasis is easily rationalized given the substantial challenges[2] in moving beyond established analytical approaches based on *two-terminal* junctions formed using scanning tunneling[3,4] or conducting atomic force microscope[5] (STM or AFM), or eutectic gallium-indium (EGaIn),[6] methods. Nonetheless, several studies have also considered transport through multi-terminal,[2,7,8] or branched,[9–11] molecular junctions, for example, seeking to influence the alignment of conducting molecular orbitals with the electrode Fermi energy (E_F), or to evaluate nanoscale circuit rules governed by quantum effects. Though certainly still a distant target, we propose that extended multi-molecular circuits may, in principle, be assembled by connecting individual components through bridging molecular nodes (in addition to, for example, bridging metal nanoparticles[12] or discreet electrodes[13]). Such nodes could serve to electronically couple each element, isolate them from each other to preserve their independent function, or serve both purposes through a reversible switching event. Accordingly, efforts to develop and evaluate the conducting properties of molecular structures that could modulate transport through well-defined two- or three-dimensional (2D or 3D) geometries are critical. Such structural elements are also of current interest for the construction of conductive, permanently porous 2D and 3D ordered polymers (OPs) such as covalent organic[14] and metal-organic frameworks (COFs and MOFs),[15] materials targeted for applications in electrochemical energy storage[16,17] or chemical sensing.[18,19] Here, for example, nodes that strongly electronically-couple appended groups may be utilized in the construction of bulk materials with large band dispersions.[15]

A prototypical class of 3D tetratopic building blocks are tetraphenylmethane and silane. Such compounds, typically with appended -SH or -CN groups, have been utilized as molecular tripods on metal surfaces, and in molecular junctions.[20–31] To improve the conductivity of these materials (albeit anisotropically), and facilitate synthetic methods that yield asymmetrical tetrapods, a *spiro* carbon core structure was developed by Mayor and coworkers.[32–34] This introduces a conjugated pathway between two of the four aryl groups. The thermoelectric properties of junctions comprising different tripodal σ-aryl metal sulfido complexes have also been probed computationally.[35] Several groups have utilized building blocks based on the methane or silane core, appended with appropriate coordinating or reactive groups such as -

$B(OH)_2$,[36] or $-NH_2$,[37] to construct 3D OPs with extended diamond-like or distinct framework structures.[38,39] However, such OPs are not known to be good electrical conductors – in part due to the broken conjugation between aryl groups at each tetrahedral node. While efforts to develop organic building blocks with improved properties are underway (e.g., featuring enhanced through-molecule conjugation),[40] electrically conductive 3D OPs are rare in comparison to their 2D counterparts.[15] Notable examples include MOFs based on $Fe(tri)_2(BF_4)_x$ (tri^- = 1,2,3-triazolate, x = 0.09-0.33)[41] and FeTHQ (tetrahydroxy-1,4-quinone)[42] complexes, and a COF comprising cyclooctatetrathiophene nodes.[43] Interestingly, such conductive systems often utilize redox-active components which are thought to improve conductivity through charge hopping transport mechanisms and/or increase the number of carriers through partial oxidation/reduction of the system (doping).[15]

In this context, replacement of the sp^3-hybridized carbon or silicon atom with a transition metal ion could improve electronic coupling between aryl groups and impart desirable redox properties to the tetraphenyl motif. Of the known air-stable metal(IV) tetraaryls,[44] the osmium(IV) complexes present an attractive target given their relatively well-established synthetic chemistry,[45–49] reversible redox chemistry at low potentials,[50] and large radially diffuse *5d* orbitals that transform with π-symmetry in a tetrahedral environment.[51] Notably, in a recent (spectro)electrochemical study of ferrocenyl-appended osmium(IV), silane, and methane complexes, spectral features attributed to intervalence-charge transfer bands for the partially oxidized osmium species were observed (a signature of electronic coupling between the $Fe^{2+/3+}$ centers).[45] Unfortunately, the degree of coupling across each different central atom could not be assessed in this work as the mixed-valence states of the silane and methane compounds proved difficult to access. These results did, however, further motivate our efforts to evaluate charge transport through analogous compounds in comparative conductance measurements, and build on the growing interest in utilizing transition metal complexes and inorganic clusters as molecular electronic components.[52,53] While such investigations have reported, for example, extraordinary conductance-distance relationships,[54,55] exotic transport behavior such as Coulomb/current blockade,[56,57] and unusual direct metal-electrode contact chemistries,[58] we recognize they should be approached with care. Synthetic challenges must often be overcome in producing an oligomeric, or modular, series of compounds, and the stability of any given complex in contact with an electrode cannot be assured.[59]

In this work we synthesize and study three families of molecules comprising tetravalent osmium (**Os-*n***), silicon (**Si-*n***), and carbon (**C-*n***) centers tetrahedrally coordinated with four

identical linker arms (**Figure 1**). Each arm comprises a conjugated oligomeric wire with n = 1-3 *para*-substituted aryl units, terminated with a thioether group for electrode binding. We show, through reproducible conductance measurements in tetradecane (TD), that junctions comprising **Os1**, **Si1**, and **C1** each exhibit a similar conductance. Junctions formed from **Os2**, in contrast, exhibit a conductance that is up to 5× higher than the organic wires. The conductance of **Os-*n*** junctions are highly variable when instead formed from 1,2,4-trichlorobenzene (TCB) solutions, suggesting these systems are particularly sensitive to the solvent environment and/or the alignment between the molecular orbitals that dominate transport and E_F. We support this hypothesis through preliminary electrochemical studies in propylene carbonate (PC) which show the conductance of **Os2** junctions can be modulated by ~45× (through bias-dependent shifts of the transmission function relative to the average E_F of the junction) and that these junctions can exhibit a >80× higher conductance than those formed from **Si2** under the same conditions. Notably, we also observe evidence of heterolytic Os-, Si-, and C-aryl bond cleavage to form Au-C(sp^2) linked junctions comprising the dissociated linker arm, showcasing a new mechanism to form these chemisorbed contacts.

To help rationalize our experimental findings, we perform gas-phase density functional theory (DFT) and DFT-based quantum transport calculations. Our results show that **Os-*n*** molecules exhibit delocalized frontier orbitals and corresponding single-molecule junctions with high conductivity, consistent with experimental observations. This behavior is associated with well-coupled frontier orbitals with energies close to E_F. Furthermore, when solvent effects are not considered, theoretical calculations suggest that **Os-*n*** junctions should be substantially more conductive than their **Si-*n*** and **C-*n*** counterparts. These findings highlight valuable opportunities for further investigation into the measurement and computation of junctions comprising tetrahedrally coordinated complex molecules, particularly in electrochemically active environments. They also motivate additional studies to refine our understanding of complex stability and frontier orbital energy alignment, addressing key challenges in the field.

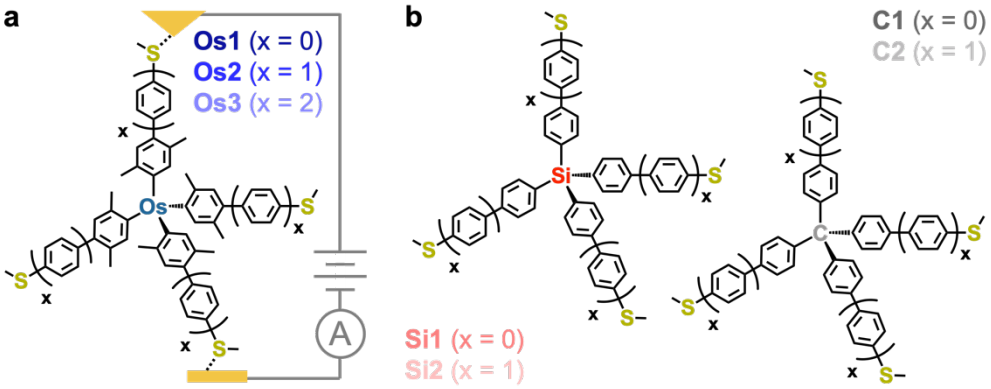

Figure 1. (a) Molecule junctions containing model tetraarylosmium(IV) complexes comprising mono, bi, or triaryl ligands terminated with thioether electrode linker groups. **(b)** Chemical structures of tetraarylsilane and tetraarylmethane analogues.

RESULTS AND DISCUSSION

The monoaryl compounds **Os1** and **Si1** were synthesized through direct reaction between aryl magnesium bromide or aryl lithium with $(Oct_4N)_2[OsBr_6]$[49,60] or $SiCl_4$,[61] respectively, whereas **C1** was prepared through nucleophilic substitution of tetrakis(4-bromophenyl)methane with sodium thiomethoxide (**Figure 2a**).[62] The oligoaryl compounds were each prepared through Suzuki cross-coupling[48] of 4-(methylthio)phenylboronic acid or 4-(4-methylthiophenyl)phenylboronic acid with tetrakis(4-bromo-2,5-dimethylphenyl)osmium(IV),[45] tetrakis(4-bromophenyl)silane, or tetrakis(4-bromophenyl)methane. All compounds were isolated as solids that readily dissolved in common organic solvents and proved air-stable even in solution. The yields of each product typically varied between 9-34% (55-76% per bond). The relatively low yield of **Si1** (2%; 21% per bond) is attributed to incomplete lithiation of the 4-bromothioanisole precursor. The compounds **Si3** and **C3** (analogous to **Os3** with Si/C central atoms) were projected to exhibit a conductance below the noise floor of our instrument so their synthesis was not pursued. While $Os(aryl)_4$ complexes are known to react with small Lewis acids such as Pme_3, isocyanides, or CO,[47] we find they do not react with the thioethers introduced here – presumably due to the steric bulk of the associated aryl group.

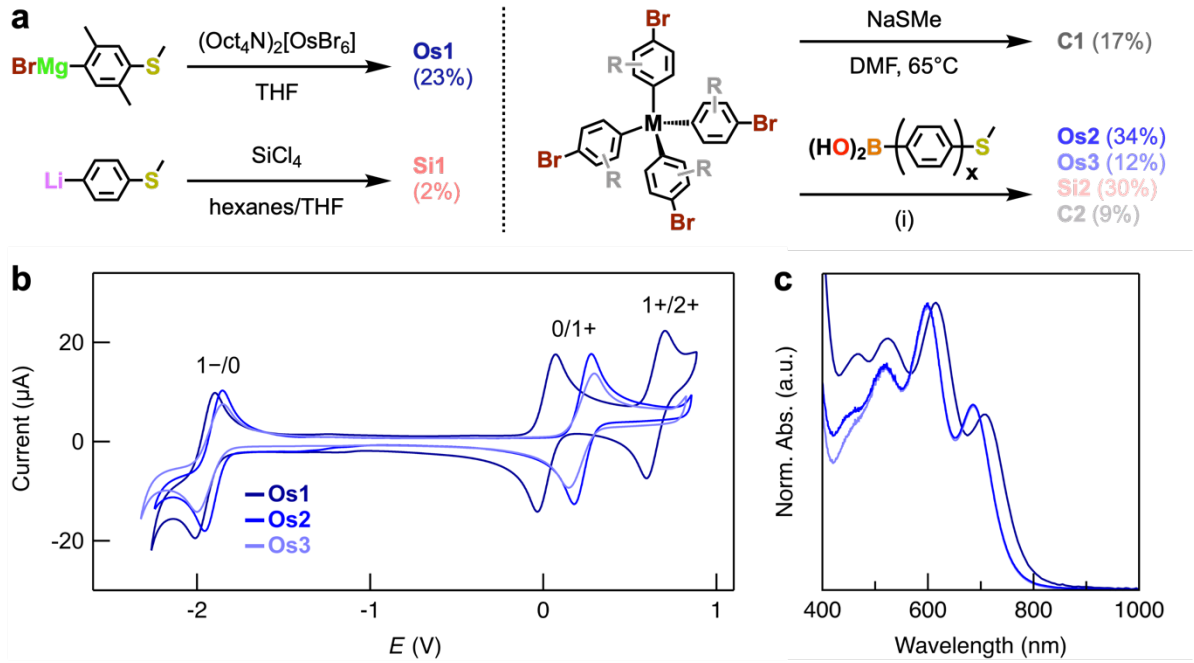

Figure 2. (a) Synthetic routes to tetraaryl compounds (x = 1, **Os2**, **Si2**, **C2**; x = 2, **Os3**). *Conditions:* (i) $Pd(PPh_3)_4$, K_2CO_3, DMF, 110°C. **(b)** Overlaid cyclic voltammograms of **Os-*n***. **(c)** Overlaid UV-vis spectra for **Os-*n***, normalized to the peak of maximum intensity in the visible region (additional spectra are provided in **Figure S1**).

The electronic properties of **Os-*n*** were probed in solution electrochemical and spectroscopic studies, given that $Os(aryl)_4$ are known to exhibit reversible redox chemistry and strongly adsorb in the visible region.[45,49,50,63,64] Data for all compounds studied is provided in **Tables S1-2**. In **Figure 2b**, we plot overlaid cyclic voltammograms for **Os-*n*** in CH_2Cl_2-$^nBu_4NPF_6$. These measurements reveal reversible redox features corresponding to 0/1+ and 1−/0 events ($i_{pa}/i_{pc} \sim 1$, $i_p \propto V_s^{1/2}$) which have previously been assigned to the $Os^{4+/5+}$ and $Os^{3+/4+}$ couples, respectively.[50] **Os1** also exhibits a 1+/2+ redox feature that has been observed for some other complexes with 4-substituted aryl ligands.[49,60] Notably, the electrochemical band gap of these materials (1.97-2.15 V) *increases* from **Os1** to **Os2** ~ **Os3** (with increasing ligand length). This trend contrasts with expectations for conjugated organic materials and reflects the critical role of the osmium *5d* orbitals in dictating the electronic properties of these wires. In **Figure 2c** we plot overlaid UV-vis spectra for **Os-*n*** that each show the four strongly absorbing bands in the visible region that are characteristic of this family of complexes.[60,63,65] Critically, the trends in optical gaps (785-757 nm, 1.58-1.64 eV) correlate with those of the electrochemical gaps, suggesting these are characteristic of the complexes themselves and are not dictated by the electrochemical environment. **Si-*n*** and **C-*n*** (n = 1-2) exhibit optical gaps

that are much larger than those of **Os-*n*** (≤335 nm, >3.7 eV) and decrease in energy with increasing ligand length (**Figure S1**).

We next perform single-molecule conductance measurements with the STM-based break junction (STM-BJ) method, using custom-built instrumentation which has been described previously.[66,67] Briefly here, we apply a voltage (V_{bias}) between a gold STM tip and gold substrate while pushing these electrodes repeatedly in and out of mechanical contact as we measure the current (I) through the junctions that are produced. Plots of conductance ($G = I/V_{bias}$) versus increasing tip-substrate displacement reveal step features at ~1 G_0 ($= 2e^2/h$) indicative of the formation of gold-gold atomic point contacts. After breaking the point contacts in the presence of molecules that can bridge the tip-substrate nanogaps, we observe additional conductance step features below 1 G_0 that we attribute to the formation of single-molecule junctions. Thousands of such conductance-displacement traces are compiled without data selection into 1D conductance histograms, whereby the step features combine to provide peaks that can be further fit with Gaussian peaks to obtain the most probable junction conductance. The data is subjected to additional analyses, for example, by constructing 2D histograms that retain the step displacement information.

In **Figure 3a-c**, we first present overlaid 1D histograms for **Os-*n***, **Si-*n***, and **C1** measured in TD, as well as **C2** measured in TCB. Under these experimental conditions, histograms show conductance peaks which are reproducible within a factor of ~2 (**Figures S2**, **S6b**). In most histograms, we observe two distinct peaks for each compound at high and low conductance. We associate each series of features with junctions formed from the parent compounds, given that the conductance of peaks from each compound family is found to systematically decrease as the number of aryl groups in each ligand increases (**Figure 3e,f**). In **Figure 3d** we present an illustrative 2D histogram for **Os2** that shows the step features corresponding to both high and low conductance junction geometries extend to ~0.5 and ~1 nm, respectively. 2D histograms for other **Os-*n***, **Si-*n***, and **C-*n*** are provided in **Figure S3** and **S6d**, which show step lengths for both high and low conductance features are similar for junctions formed from compounds with linker arms comprising the same number of aryl groups, even when these are connected to different central atoms.

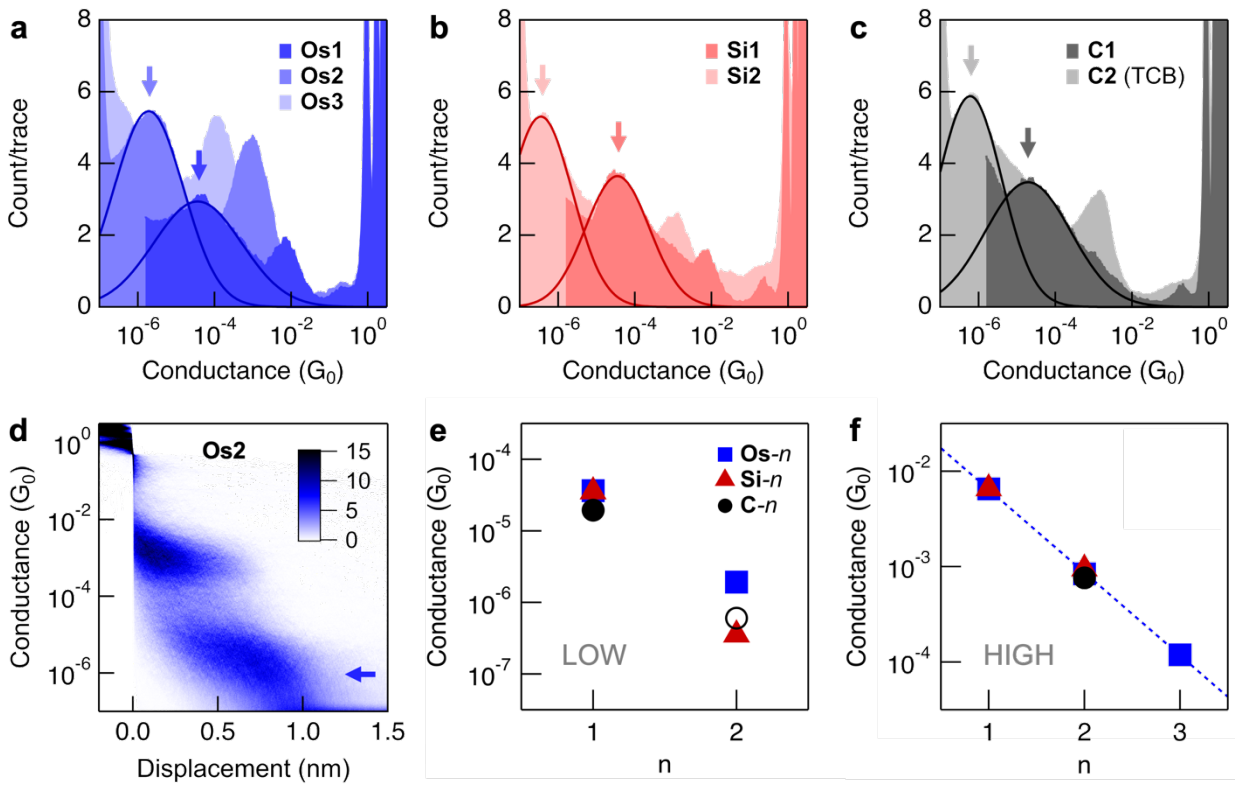

Figure 3. Overlaid 1D histograms for **(a) Os-*n***, **(b) Si-*n***, **(c) C-*n*** (≥5,000 traces). All measurements were performed with V_{bias} = 750 mV in TD, except for studies of **Os1**, **Si1**, and **C1** which used V_{bias} = 250 mV, and **C2** which was measured in TCB. Arrows mark the low conductance features assigned to junction geometries where compounds are linked to each electrode by a single thioether anchor (1:1 configuration, **Figure 1a**). **(d)** 2D conductance histogram for **Os2**. Additional 2D histograms are provided in **Figure S3**, **S6d**. **I** A plot of peak conductance versus *n* for the low conductance feature. All data is from measurements in TD (solid), except for **C2** which was measured in TCB (hollow). **(f)** A plot of peak conductance versus *n* for the high conductance peak feature observed in each series of wires measured in TD. A fit of conductance versus *n* for the high conductance peak of **Os-*n*** using $G = G_c \cdot \exp(-\beta n)$ gives $\beta = 2.0/n$ (dashed line).

Focusing first on the low conductance features, we note that their maximum displacement is close to the calculated S-S distance for each compound obtained from DFT-optimized structures after accounting for the gold snapback distance of ~0.6 nm.[68,69] For **Os1**, **Si1**, and **C1**, step displacement is ~0.4 nm and the calculated S-S distances are ~1.1 nm (**Figure S3**). For **Os2**, **Si2**, and **C2** the step displacement is ~1 nm and the calculated S-S distances are 1.7-1.9 nm (**Figures 3d**, **S3d**, **S6d**). Accordingly, we attribute the low conductance features to junctions comprising a tetrahedrally-coordinated central atom linked to each electrode by one anchor group (the 1:1 configuration; **Figure 1a**). In support of this assignment, we note the conductance observed for **Si1** (3.5×10^{-5} G_0 at V_{bias} = 250 mV in TD) is comparable to the

reported conductance of the structurally similar $SiMe_2(C_6H_4\text{-}SMe)_2$ (~7×10^{-5} G_0 at V_{bias} = 225 mV in TCB; which only comprises two linker groups to form junctions).[70] While we cannot rule out the formation of junctions linked to either electrode by two or three thioether anchors, we suggest such 1:2, 1:3, or 2:2 configurations are less probable, exhibit comparable conductance to junctions linked by a single anchor on each electrode, or are already captured in measurements at smaller junction displacements prior to breaking the molecular junction (accounting in part for the highly sloped conductance-displacement features observed). In **Figure 3e**, a plot of peak conductance against *n* for the low conductance features reveals that the conductance of **Os1**, **Si1**, and **C1** are comparable. In contrast, **Os2** exhibits a higher conductance than **Si2** in TD and **C2** in TCB by factors of ~5 and ~3, respectively. Conductance data are provided in **Table S3**.

As the maximum displacement of each high conductance step is approximately half of the displacement observed for the low conductance step, we propose this feature may be attributed to junctions comprising linker arms that have been cleaved at the central atom-aryl bond. In support of this hypothesis, we plot, in **Figure 3f**, peak conductance versus *n* for the high conductance features observed in each family of compounds (see **Figure S7** for the same plot using data from TCB measurements). A fit to the data for **Os-*n*** provides a tunneling decay constant, β, of 2.0/*n*, close to values typically found for wires with oligoaryl backbones.[4,71] Furthermore, the conductance of the high conductance peaks is independent of the central atom of the molecular precursor used. Our assignment of this histogram feature is further supported by the observation that the junctions formed from complexes with biphenyl ligands exhibit a similar conductance to those formed from 4'-(methylthio)-[1,1'-biphenyl]-4-yl)(triphenylphosphine)gold(I), a complex comprising the same ligand with a pre-installed gold-carbon bond (see **Figure S8** and supporting discussion). In **Figure S9** we propose a tentative reaction scheme to rationalize these observations. We propose that tetraaryl compounds undergo heterolytic central atom-aryl bond cleavage to provide a stable trityl (with carbon),[72] or trityl-like (with silicon[73] or osmium), cation and a corresponding nucleophilic aryl anion. Such an anion could feasibly form junctions linked on one side through an Au-C(sp^2) bond, and on the other through the thioether. This hypothesis follows recent reports that show organic wires comprising aryl-S^{t}Bu groups can form junctions comprising chemisorbed S-Au linkages, apparently with loss of the stable *tert*-butyl carbocation.[74,75]

For completeness, we note that the histogram of **Os3** in TD does not feature a low conductance peak, likely because the conductance of junctions bound to each electrode with thioanisole anchors (comprising six aryl groups) falls below the minimum conductance limit

of our current instrumentation. Furthermore, in **Figure 3c** we present a conductance histogram from measurements of **C2** in TCB because studies of this molecule in TD have so far not provided the expected low conductance peak (**Figure S4**). We recognize that this feature would be absent in measurements where the rate of ligand dissociation increased to a critical value that disrupted the formation of junctions linked by thioether anchors to each electrode.

While measurements of **C2** in TCB proved useful in this context, we have focused our discussion on STM-BJ studies with TD due to significant experimental variations observed for low conductance junctions of **Os-*n*** measured in TCB. In the examples provided in **Figure S5**, the low conductance feature of **Os2** varies by a factor of ~8, up to 1.4×10^{-5} G_0 (an order of magnitude higher than the conductance measured in TD). In some experiments, it appears that **Os3** junctions of the 1:1 configuration can be observed above our instrument noise floor. While we cannot yet provide a firm rationale for these observations, we suggest that the use of TCB, despite its widespread utilization in single-molecule conductance experiments, has the potential to complicate studies of chemically sensitive or redox-active compounds (particularly under applied electric fields near the junction). Other chlorinated solvents such as $CDCl_3$ or CH_2Cl_2 can prove weakly acidic due to the photogeneration of HCl,[76] or may oxidize compounds with low redox potentials such as ferrocene through charge transfer to solvent (CTTS) optical transitions.[77] Aromatic chlorinated solvents are also known to interact with a gold surface to a limited degree, influencing frontier orbital-E_F level alignment.[78] The greater consistency of conductance measurements in TD may accordingly be attributed to the non-polar, inert character of this solvent, which inhibits the dissolution of charged species and does not strongly interact with the gold surface.

To help further rationalize the potential for **Os-*n*** junctions to vary in conductance with level alignment or through *in situ* oxidation, we perform conductance measurements of **Os2** in propylene carbonate (PC). In such experiments, it is essential to use a wax-coated tip to minimize background Faradaic and capacitive currents that would otherwise obscure junction tunneling currents of interest.[79] However, as the exposed tip electrode area (~1 μm) is small relative to the area of the substrate electrode (~1 cm^2), this also results in the generation of a dense double-layer at the tip that is thought to induce a bias-dependent shift of the transmission function relative to the average E_F of the junction.[80] As a result, the bias window opens asymmetrically about E_F, enabling experiments that probe the transmission landscape for different molecules,[80] establish whether the dominant conducting orbital is occupied or unoccupied,[80,81] or construct junctions that exhibit significant current rectification.[82]

In **Figure 4a**,**b** we present overlaid 1D histograms for **Os2** measured in PC at different tip-substrate biases across two separate experiments which show that the conductance of the junctions formed can be modulated by a factor of 47, increasing as V_{bias} is made more positive. The representative 2D histograms shown in **Figure 4d**,**e** confirm that the junction conductance increases while the maximum junction displacement remains constant. These observations are consistent with a sloped transmission near E_F, and indicate that transport through **Os2** junctions is HOMO-dominated, as is also found in the calculations discussed below. In contrast, we observe the peak attributed to junctions comprising dissociated ligand does not significantly change in conductance with applied bias and reduces in intensity for tip biases more positive than −250 mV. In **Figure 4c**, we provide a cyclic voltammogram of **Os2** obtained *in situ* using the gold STM tip as working electrode and the substrate as both reference and counter electrode (obtained during experiment 2, shown in **Figure 4b**). This shows a redox wave close to ~0.8 V that we assign to the 0/1+ event observed for this compound (**Figure 2b**), confirming that we approach the HOMO resonance as we apply a more positive V_{bias}. We find that we cannot easily form junctions for $V_{bias} > +700$ mV; similar limits have been observed in studies of other molecules with resonances close to E_F.[80] Finally, in **Figure 4f**, we plot peak conductance versus V_{bias} (using Gaussian fits to the histogram peaks in **Figure 4a** and **b)**, further illustrating the consistent increase in conductance with increasing positive V_{bias} and the reproducibility of conductance values between different experiments. Together, these studies support the view that variations in level alignment could indeed result in significant changes to the conductance of **Os-*n*** junctions, on the order of those observed in repeated measurements in TCB. Analogous PC measurements performed using **Si2** show a much smaller change in conductance with V_{bias} (**Figure 4f, S10**), consistent with a transmission function that is flat around E_F. At $V_{bias} = +700$ mV, the conductance of **Si2** junctions is 83× smaller than that those formed from **Os2**, clearly illustrating the distinct electronic structures of these compounds.

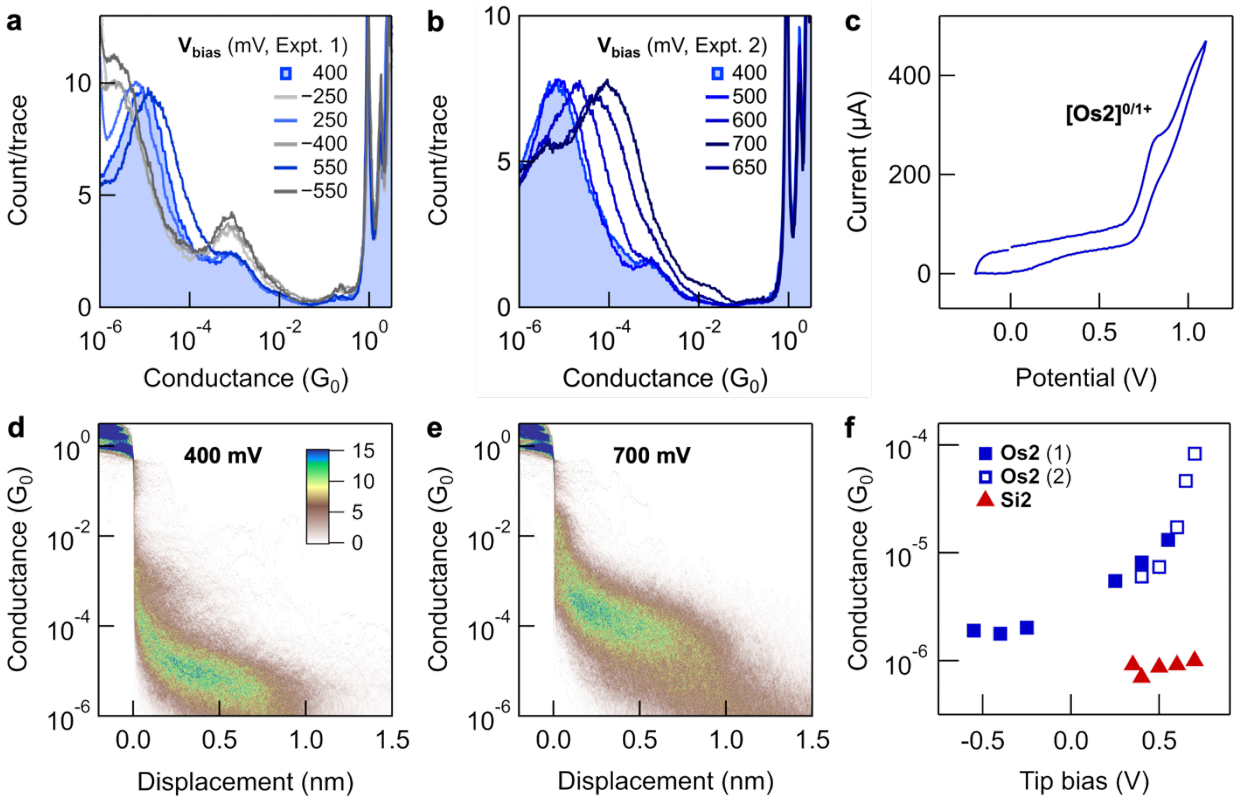

Figure 4. (a,b) Overlaid 1D histograms (2,000 traces) for measurements of **Os2** in PC at different V_{bias}, across two different experiments (biases listed in chronological order). This data shows that junction conductance can increase by a factor of 47 with changing V_{bias}. **I** Cyclic voltammogram obtained using the same tip, substrate, and solution as used for the STM-BJ measurements in panel (b) with an external potentiostat. Here the wax-coated STM tip served as the working electrode, the substrate as both the counter and reference electrodes. **(d,e)** 2D histograms obtained for measurements at V_{bias} = +400 mV and +700 mV, respectively, corresponding to the 1D histograms in panel (b). **(f)** A plot of peak conductance versus V_{bias} for the measurements of **Os2** shown in panels (a) and (b) (blue). An overlaid plot for PC measurements of **Si2** show these junctions exhibit a much smaller dependance on V_{bias} (red; see **Figure S10** for corresponding histograms).

To gain insight into the charge transfer properties of these junctions, we now turn to quantum transport calculations. Our transport calculations are based on density functional theory (DFT) and the non-equilibrium Green's functions formalism, and are performed using the combination of FHI-aims[83] and the transport module AITRANSS.[84–86] Additional computational details can be found in the **SI**. We show, in **Figure 5a**, overlaid transmission functions for **Os-*n***, bound to gold electrodes with two thioether linkers. An example of these relaxed junction geometries is given in **Figure 5c**. We observe that the conductance, which is proportional to the transmission at E_F, is highest for the smallest complex and follows the trend: **Os1** > **Os2** > **Os3**. This behavior appears counterintuitive when considering the trend observed

in the HOMO-LUMO gaps for the isolated molecules (see **Table S8** for calculated values, which qualitatively agree with those found through experiment), and in which shorter wires typically exhibit larger HOMO-LUMO gaps. Here, the conductance ordering is attributed to the alignment of the HOMO level with E_F, along with its decreasing width as the wire length increases. As is common in calculations using semi-local functionals, the computed conductance of **Os-*n*** is overestimated by more than an order of magnitude compared to experiment, a well-understood artifact arising from the limitations of generalized-gradient approximations to DFT functionals.[87,88] Notably, the calculated conductance of **Os3** is very low, consistent with experimental observations where it falls below the noise level.

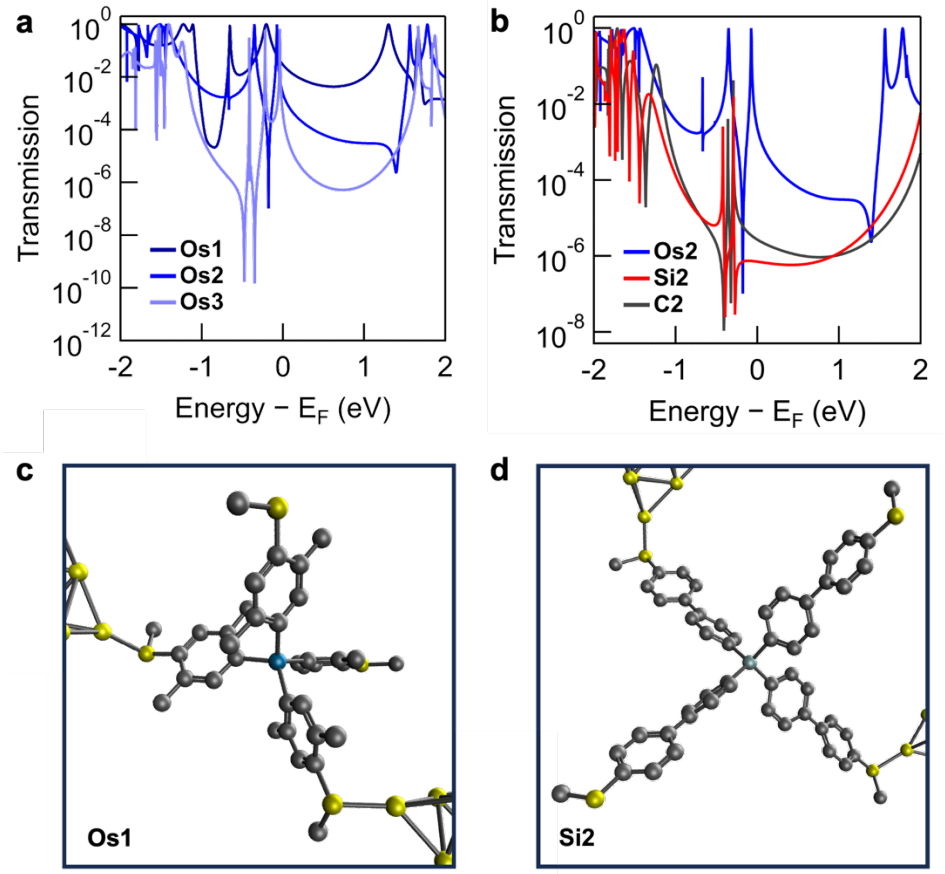

Figure 5. (a) Overlaid transmission functions for the **Os-*n*** series. **(b)** Comparison of overlaid transmission functions for **Os2**, **Si2**, and **C2** (data for **Os2** reproduced from panel (a)). **(c-d)** Optimized geometries of **Os1** and **Si2** junctions, respectively. Hydrogen atoms excluded for clarity.

We have also performed quantum transport calculations for the **Si-*n*** and **C-*n*** molecular junction series. In **Figure 5b** we show a comparison of the transmission functions for $n = 2$ (**Os2**, **Si2**, **C2**), additional results for the entire **Si-*n*** and **C-*n*** series are available in **Figure S15**.

An example of one of these relaxed junction geometries is shown in **Figure 5c**. We recognize that all these junctions exhibit complex transmission functions with Fano-type interference features, which can be attributed to the existence of non-bonded aryl groups in the complexes. The calculated conductance of **Si-*n*** and **C-*n*** follows the same trend as **Os-*n***, with **Si1** > **Si2** > **Si3** and the same ordering for **C-*n***. However, in this case, the trend aligns with the expected behavior based on the HOMO-LUMO gaps, indicating that these molecules, in general, behave as conventional molecular wires. Additionally, the calculated HOMO-LUMO gaps of **Si-*n*** and **C-*n*** are very similar and substantially larger than those of **Os-*n*** with a difference of 1–2 eV between **Os-*n*** and **Si-*n*/C-*n*** (**Table S8**). Our transport calculations show that **Os2** is HOMO conducting and exhibits a significantly higher conductance than **Si2/C2**, though the exact difference may change due differences in E_F alignment and solvent effects. This qualitatively aligns with experimentally measurements in PC at V_{bias} = +700 mV which show that **Si2** is ~80× less conductive than **Os2**, with the conductance of **Os2** junctions increasing ~45× under changing bias. Our calculations for **Si2** also recover the flatness of the transmission function close to E_F as suggested by these experimental measurements. It is important to note that our calculations do not account for the effects of solvents or electrochemical influences. This limitation could offer a possible explanation for some discrepancies between the theoretical results and experimental observations.

In closing, we note that calculated tunnel couplings, which are related to conductance,[4,89] align well with the DFT transmission calculations in **Figure 5**, consistently recovering highly conductive **Os-*n*** junctions (**SI**, *Tunnel Coupling*). While differences in the orientation of adjacent aryl rings connected through the central atom can lead to variations in tunnel couplings due to non-equivalent geometries (which we define, in **Figure S11**, using pairs of dihedral angles), these differences do not significantly affect the calculated transmission when larger gold clusters are used to model the reservoirs (**Figure S16**). Additionally, tunnel coupling calculations using the B3LYP functional suggest that the differences between **Os-*n***, **Si-*n***, and **C-*n*** junctions may be smaller than those predicted by PBE (**Table S6,7**), providing further insight into the influence of exchange-correlation effects on transport properties.

CONCLUSION

In this study we have evaluated the conductance of single-molecule junctions formed from tetraaryl compounds comprising osmium, silicon, or carbon central atoms. Remarkably, for

most molecules studied in TD, we find evidence for heterolytic central atom-aryl bond cleavage reactions to form gold-(aryl)$_n$-S(Me)-gold junctions comprising Au-C(sp^2) contacts. This observation is consistent with reports that chemisorbed Au-S junction linkages may be formed *in situ* through the loss of stable *tert*-butyl carbocations,[75,74] recognizing that the corresponding trityl or trityl-like cations formed are also known to exhibit a high stability.[72] Extrapolating this concept, we suggest that the preinstallation of stable carbocation precursors may provide a general strategy to form other chemisorbed junction contact chemistries. Perhaps surprisingly, conductance features assigned to junctions comprising intact compounds with different central atoms exhibit highly comparable conductance values when formed in TD – except for **Os2** which yields a 4-6× higher conductance. We speculate, based on the variability of **Os-*n*** measurements in TCB, as well as the highly tunable conductance of **Os2** junctions in electrolytic environments (relative to those with **Si2**), that the conductance of these organometallic wires may generally be increased by varying their charge state or surrounding solvent environment.

In this context, we reaffirm that solution-based electrochemical and spectroscopic studies show that **Os-*n*** have smaller HOMO-LUMO gaps than **Si-*n*** or **C-*n*** compounds, which could improve frontier orbital-E_F energy level alignment. Transmission calculations using a semi-local functional further indicate that **Os-*n*** junctions exhibit smaller HOMO-LUMO gaps with broad, well-coupled transmission resonances, compared to **Si-*n*** and **C-*n*** junctions. Together, our results underscore the potential of these complexes for high-conductance applications while also highlighting the need for further investigation into the stability and structure of osmium complexes captured and measured between gold electrodes. Despite exhibiting a remarkable air-stability in solution, Os(aryl)$_4$ are known to undergo a range of reactions *ex situ* to form distinct compounds, for example, comprising oxo or η^6-biaryl ligands, including OsO(aryl)$_4$,[64] OsO$_2$(aryl)$_2$,[90] or Os(η^6-biaryl)(aryl)$_2$(L) (previously isolated with L = Pme$_3$, CO).[47] Subsequent studies are needed to evaluate methods that might stabilize the parent **Os-*n*** complexes during STM-BJ studies, and to probe the conductance of different osmium σ-aryl compounds synthesized *ex situ* to assess the possibility of their formation *in situ*.

ASSOCIATED CONTENT

Electronic Supplementary Information (ESI) available: Additional synthetic, spectroscopic, conductance, and computational details and data. This includes synthetic procedures, 1D and

2D conductance histograms, transmission calculations, and ^{1}H and $^{13}C\{^{1}H\}$ NMR spectra for all new compounds.

AUTHOR INFORMATION

Corresponding Author

Michael S. Inkpen – Email: inkpen@usc.edu

Daniel Hernangómez-Pérez – Email: d.hernangomez@nanogune.eu

Notes

The authors declare no competing financial interest.

ACKNOWLEDGEMENTS

This work was primarily supported by funding from the University of Southern California (USC) and the National Science Foundation (NSF CAREER Award to M.S.I., CHE-2239614). D. H.-P. is grateful for funding from the Diputación Foral de Gipuzkoa through Grants 2023-FELL-000002-01, 2024-FELL-000009-01. Instrumentation in the USC Chemistry Instrument Facility was acquired with support from the USC Research and Innovation Instrumentation Award Program. Additionally, funds provided by the NSF (DBI-0821671, CHE-0840366) and National Institute of Health (S10 RR25432) supported the acquisition of the NMR spectrometers used in our work.

REFERENCES

(1) Su, T. A.; Neupane, M.; Steigerwald, M. L.; Venkataraman, L.; Nuckolls, C. Chemical Principles of Single-Molecule Electronics. *Nat. Rev. Mater.* **2016**, *1* (3), 16002. https://doi.org/10.1038/natrevmats.2016.2.

(2) Xiang, D.; Jeong, H.; Kim, D.; Lee, T.; Cheng, Y.; Wang, Q.; Mayer, D. Three-Terminal Single-Molecule Junctions Formed by Mechanically Controllable Break Junctions with Side Gating. *Nano Lett.* **2013**, *13* (6), 2809–2813. https://doi.org/10.1021/nl401067x.

(3) Xu, B.; Tao, N. J. Measurement of Single-Molecule Resistance by Repeated Formation of Molecular Junctions. *Science* **2003**, *301* (5637), 1221–1223.

(4) Venkataraman, L.; Klare, J. E.; Nuckolls, C.; Hybertsen, M. S.; Steigerwald, M. L. Dependence of Single-Molecule Junction Conductance on Molecular Conformation. *Nature* **2006**, *442* (7105), 904–907. http://www.nature.com/nature/journal/v442/n7105/suppinfo/nature05037_S1.html.

(5) Wold, D. J.; Frisbie, C. D. Formation of Metal-Molecule-Metal Tunnel Junctions: Microcontacts to Alkanethiol Monolayers with a Conducting AFM Tip. *J Am Chem Soc* **2000**, *122*, 2970–2971.
(6) Chiechi, R. C.; Weiss, E. A.; Dickey, M. D.; Whitesides, G. M. Eutectic Gallium–Indium (EGaIn): A Moldable Liquid Metal for Electrical Characterization of Self-Assembled Monolayers. *Angew. Chem. Int. Ed.* **2008**, *47* (1), 142–144. https://doi.org/10.1002/anie.200703642.
(7) Fu, H.; Zhu, X.; Li, P.; Li, M.; Yang, L.; Jia, C.; Guo, X. Recent Progress in Single-Molecule Transistors: Their Designs, Mechanisms and Applications. *J. Mater. Chem. C* **2022**, *10* (7), 2375–2389. https://doi.org/10.1039/D1TC04079K.
(8) Neuhauser, D.; Baer, R. Phase Coherent Electronics: A Molecular Switch Based on Quantum Interference. *J Am Chem Soc* **2002**, *124* (16), 4200–4201.
(9) Vazquez, H.; Skouta, R.; Schneebeli, S.; Kamenetska, M.; Breslow, R.; Venkataraman, L.; Hybertsen, M. S. Probing the Conductance Superposition Law in Single-Molecule Circuits with Parallel Paths. *Nat Nanotechnol* **2012**, *7* (10), 663–667. http://www.nature.com/nnano/journal/v7/n10/abs/nnano.2012.147.html#supplementary-information.
(10) Magoga, M.; Joachim, C. Conductance of Molecular Wires Connected or Bonded in Parallel. *Phys Rev B Solid State* **1999**, *59* (24), 16011–16021.
(11) Błaszczyk, A.; Chadim, M.; von Hänisch, C.; Mayor, M. Synthesis of Macrocyclic Molecular Rods as Potential Electronic Devices. *Eur J Org Chem* **2006**, *2006* (17), 3809–3825. https://doi.org/10.1002/ejoc.200600336.
(12) Cui, X. D.; Primak, A.; Zarate, X.; Tomfohr, J.; Sankey, O. F.; Moore, A. L.; Moore, T. A.; Gust, D.; Harris, G.; Lindsay, S. M. Reproducible Measurement of Single-Molecule Conductivity. *Science* **2001**, *294* (5542), 571–574. https://doi.org/10.1126/science.1064354.
(13) Byeon, S. E.; Kang, H.; Yoon, H. J. Toward Printed Molecular Electronics: Direct Printing of Liquid Metal Microelectrode on Self-Assembled Monolayers. *Adv. Electron. Mater.* **2021**, *7* (2), 2000829. https://doi.org/10.1002/aelm.202000829.
(14) Jin, E.; Asada, M.; Xu, Q.; Dalapati, S.; Addicoat, M. A.; Brady, M. A.; Xu, H.; Nakamura, T.; Heine, T.; Chen, Q.; Jiang, D. Two-Dimensional Sp2 Carbon–Conjugated Covalent Organic Frameworks. *Science* **2017**, *357* (6352), 673–676.
(15) Xie, L. S.; Skorupskii, G.; Dincă, M. Electrically Conductive Metal–Organic Frameworks. *Chem. Rev.* **2020**, *120* (16), 8536–8580. https://doi.org/10.1021/acs.chemrev.9b00766.
(16) Zhang, Y.; Riduan, S. N.; Wang, J. Redox Active Metal- and Covalent Organic Frameworks for Energy Storage: Balancing Porosity and Electrical Conductivity. *Chem. - Eur. J.* **2017**, *23* (65), 16419–16431. https://doi.org/10.1002/chem.201702919.
(17) Calbo, J.; Golomb, M. J.; Walsh, A. Redox-Active Metal–Organic Frameworks for Energy Conversion and Storage. *J. Mater. Chem. A* **2019**, *7* (28), 16571–16597. https://doi.org/10.1039/C9TA04680A.
(18) Kreno, L. E.; Leong, K.; Farha, O. K.; Allendorf, M.; Van Duyne, R. P.; Hupp, J. T. Metal–Organic Framework Materials as Chemical Sensors. *Chem. Rev.* **2012**, *112* (2), 1105–1125. https://doi.org/10.1021/cr200324t.
(19) Meng, Z.; Stolz, R. M.; Mendecki, L.; Mirica, K. A. Electrically-Transduced Chemical Sensors Based on Two-Dimensional Nanomaterials. *Chem. Rev.* **2019**, *119* (1), 478–598. https://doi.org/10.1021/acs.chemrev.8b00311.
(20) Šebera, J.; Lindner, M.; Gasior, J.; Mészáros, G.; Fuhr, O.; Mayor, M.; Valášek, M.; Kolivoška, V.; Hromadová, M. Tuning the Contact Conductance of Anchoring

Groups in Single Molecule Junctions by Molecular Design. *Nanoscale* **2019**, *11* (27), 12959–12964. https://doi.org/10.1039/c9nr04071d.
(21) Valášek, M.; Mayor, M. Spatial and Lateral Control of Functionality by Rigid Molecular Platforms. *Chem. - Eur. J.* **2017**, *23* (55), 13538–13548. https://doi.org/10.1002/chem.201703349.
(22) Yao, Y.; Tour, J. M. Facile Convergent Route to Molecular Caltrops. *J. Org. Chem.* **1999**, *64* (6), 1968–1971. https://doi.org/10.1021/jo982085g.
(23) Zhu, L.; Harima, Y.; Yamashita, K.; Tang, H.; Hirayama, D.; Aso, Y.; Otsubo, T. Electrochemical Properties of Self-Assembled Monolayers of Tripod-Shaped Molecules and Their Applications to Organic Light-Emitting Diodes. *Chem. Commun.* **2001**, No. 18, 1830–1831. https://doi.org/10.1039/b105922j.
(24) Hirayama, D.; Takimiya, K.; Aso, Y.; Otsubo, T.; Hasobe, T.; Yamada, H.; Imahori, H.; Fukuzumi, S.; Sakata, Y. Large Photocurrent Generation of Gold Electrodes Modified with [60]Fullerene-Linked Oligothiophenes Bearing a Tripodal Rigid Anchor. *J. Am. Chem. Soc.* **2002**, *124* (4), 532–533. https://doi.org/10.1021/ja016703d.
(25) Wei, L.; Padmaja, K.; Youngblood, W. J.; Lysenko, A. B.; Lindsey, J. S.; Bocian, D. F. Diverse Redox-Active Molecules Bearing Identical Thiol-Terminated Tripodal Tethers for Studies of Molecular Information Storage. *J. Org. Chem.* **2004**, *69* (5), 1461–1469. https://doi.org/10.1021/jo0349476.
(26) Wei, L.; Tiznado, H.; Liu, G.; Padmaja, K.; Lindsey, J. S.; Zaera, F.; Bocian, D. F. Adsorption Characteristics of Tripodal Thiol-Functionalized Porphyrins on Gold. *J. Phys. Chem. B* **2005**, *109* (50), 23963–23971. https://doi.org/10.1021/jp0537005.
(27) Ie, Y.; Hirose, T.; Yao, A.; Yamada, T.; Takagi, N.; Kawai, M.; Aso, Y. Synthesis of Tripodal Anchor Units Bearing Selenium Functional Groups and Their Adsorption Behaviour on Gold. *Phys Chem Chem Phys* **2009**, *11* (25), 4949–4951. https://doi.org/10.1039/b906286f.
(28) Lindner, M.; Valášek, M.; Homberg, J.; Edelmann, K.; Gerhard, L.; Wulfhekel, W.; Fuhr, O.; Wächter, T.; Zharnikov, M.; Kolivoška, V.; Pospíšil, L.; Mészáros, G.; Hromadová, M.; Mayor, M. Importance of the Anchor Group Position (Para versus Meta) in Tetraphenylmethane Tripods: Synthesis and Self-Assembly Features. *Chem. - Eur. J.* **2016**, *22*, 13218–13235. https://doi.org/10.1002/chem.201602019.
(29) Valášek, M.; Lindner, M.; Mayor, M. Rigid Multipodal Platforms for Metal Surfaces. *Beilstein J. Nanotechnol.* **2016**, *7* (1), 374–405. https://doi.org/10.3762/bjnano.7.34.
(30) Sebechlebská, T.; Šebera, J.; Kolivoška, V.; Lindner, M.; Gasior, J.; Mészáros, G.; Valášek, M.; Mayor, M.; Hromadová, M. Investigation of the Geometrical Arrangement and Single Molecule Charge Transport in Self-Assembled Monolayers of Molecular Towers Based on Tetraphenylmethane Tripod. *Electrochimica Acta* **2017**, *258*, 1191–1200. https://doi.org/10.1016/j.electacta.2017.11.174.
(31) Kolivoška, V.; Šebera, J.; Sebechlebská, T.; Lindner, M.; Gasior, J.; Mészáros, G.; Mayor, M.; Valášek, M.; Hromadová, M. Probabilistic Mapping of Single Molecule Junction Configurations as a Tool to Achieve the Desired Geometry of Asymmetric Tripodal Molecules. *Chem. Commun.* **2019**, *55* (23), 3351–3354. https://doi.org/10.1039/c8cc09681c.
(32) Šebera, J.; Kolivoška, V.; Valášek, M.; Gasior, J.; Sokolová, R.; Mészáros, G.; Hong, W.; Mayor, M.; Hromadová, M. Tuning Charge Transport Properties of Asymmetric Molecular Junctions. *J. Phys. Chem. C* **2017**, acs.jpcc.7b01105. https://doi.org/10.1021/acs.jpcc.7b01105.
(33) Karimi, M. A.; Bahoosh, S. G.; Valášek, M.; Bürkle, M.; Mayor, M.; Pauly, F.; Scheer, E.; Agraït, N.; Cuevas, J. C.; Mikkelsen, K. V. Identification of the Current

Path for a Conductive Molecular Wire on a Tripodal Platform. *Nanoscale* **2016**, *8* (20), 10582–10590. https://doi.org/10.1039/C5NR08708B.
(34) Gerhard, L.; Edelmann, K.; Homberg, J.; Valášek, M.; Bahoosh, S. G.; Lukas, M.; Pauly, F.; Mayor, M.; Wulfhekel, W. An Electrically Actuated Molecular Toggle Switch. *Nat. Commun.* **2017**, *8*, 14672.
(35) Al-Owaedi, O. A.; Najeeb, H. N.; Aldulaimi, A. K. O.; Alwan, N. H.; Ali, M. S.; Dwech, M. H.; AL-Da'amy, M. A. Thermoelectric Signature of D-Orbitals in Tripod-Based Molecular Junctions. *Mater. Adv.* **2024**, 10.1039.D4MA00646A. https://doi.org/10.1039/D4MA00646A.
(36) El-Kaderi, H. M.; Hunt, J. R.; Mendoza-Cortés, J. L.; Côté, A. P.; Taylor, R. E.; O'Keeffe, M.; Yaghi, O. M. Designed Synthesis of 3D Covalent Organic Frameworks. *Science* **2007**, *316* (5822), 268–272. https://doi.org/10.1126/science.1139915.
(37) Uribe-Romo, F. J.; Hunt, J. R.; Furukawa, H.; Klöck, C.; O'Keeffe, M.; Yaghi, O. M. A Crystalline Imine-Linked 3-D Porous Covalent Organic Framework. *J. Am. Chem. Soc.* **2009**, *131* (13), 4570–4571. https://doi.org/10.1021/ja8096256.
(38) Zaręba, J. K. Tetraphenylmethane and Tetraphenylsilane as Building Units of Coordination Polymers and Supramolecular Networks – A Focus on Tetraphosphonates. *Inorg. Chem. Commun.* **2017**, *86*, 172–186. https://doi.org/10.1016/j.inoche.2017.10.013.
(39) Guan, X.; Chen, F.; Fang, Q.; Qiu, S. Design and Applications of Three Dimensional Covalent Organic Frameworks. *Chem. Soc. Rev.* **2020**, *49* (5), 1357–1384. https://doi.org/10.1039/C9CS00911F.
(40) Wu, M.; Shan, Z.; Wang, J.; Gu, Z.; Wu, X.; Xu, B.; Zhang, G. Three-Dimensional Covalent Organic Frameworks Based on a π-Conjugated Tetrahedral Node. *Chem. Commun.* **2021**, *57* (80), 10379–10382. https://doi.org/10.1039/D1CC03219D.
(41) Park, J. G.; Aubrey, M. L.; Oktawiec, J.; Chakarawet, K.; Darago, L. E.; Grandjean, F.; Long, G. J.; Long, J. R. Charge Delocalization and Bulk Electronic Conductivity in the Mixed-Valence Metal–Organic Framework Fe(1,2,3-Triazolate) $_2(BF_4)_x$. *J. Am. Chem. Soc.* **2018**, *140* (27), 8526–8534. https://doi.org/10.1021/jacs.8b03696.
(42) Chen, G.; Gee, L. B.; Xu, W.; Zhu, Y.; Lezama-Pacheco, J. S.; Huang, Z.; Li, Z.; Babicz, J. T.; Choudhury, S.; Chang, T.-H.; Reed, E.; Solomon, E. I.; Bao, Z. Valence-Dependent Electrical Conductivity in a 3D Tetrahydroxyquinone-Based Metal–Organic Framework. *J. Am. Chem. Soc.* **2020**, *142* (51), 21243–21248. https://doi.org/10.1021/jacs.0c09379.
(43) Wang, S.; Da, L.; Hao, J.; Li, J.; Wang, M.; Huang, Y.; Li, Z.; Liu, Z.; Cao, D. A Fully Conjugated 3D Covalent Organic Framework Exhibiting Band-like Transport with Ultrahigh Electron Mobility. *Angew. Chem. Int. Ed.* **2021**, *60* (17), 9321–9325. https://doi.org/10.1002/anie.202100464.
(44) Koschmieder, S. U.; Wilkinson, G. Homoleptic and Related Aryls of Transition Metals. *Polyhedron* **1991**, *10* (2), 135–173.
(45) Zagami, L.; Saal, T.; Avedian, C.; Inkpen, M. S. Intervalence Charge Transfer in an Osmium(IV) Tetra(Ferrocenylaryl) Complex. *Inorg. Chem.* **2025**, DOI: 10.1021/acs.inorgchem.4c04481.
(46) Tooze, R. P. Synthesis and X-Ray Crystal Structures of the First Tetrahedral Osmium(Iv) Com- Pounds, Tetrakis(Cyclohexyl)Osmium(Lv) and Tetrakis(o-Methylphenyl)Osmium(Iv).
(47) Arnold, J.; Wilkinson, G.; Hussain, B.; Hursthouse, M. B. Reactivity of the Homoleptic Osmium Aryl Os(2-MeC6H4)4: Ligand-Induced Reductive Coupling,

.Sigma.- to .Pi.-Rearrangement, and Ortho-Hydrogen Activation. *Organometallics* **1989**, *8* (5), 1362–1369. https://doi.org/10.1021/om00107a035.
(48) Lau, M.-K.; Zhang, Q.-F.; Chim, J. L. C.; Wong, W.-T.; Leung, W.-H. Direct Functionalisation of σ-Aryl Ligands: Preparation of Homoleptic Functionalised Aryls of Osmium(Iv). *Chem. Commun.* **2001**, *79* (16), 1478–1479. https://doi.org/10.1039/b104075h.
(49) Parr, J. M.; Olivar, C.; Saal, T.; Haiges, R.; Inkpen, M. S. Pushing Steric Limits in Osmium(IV) Tetraaryl Complexes. *Dalton Trans.* **2022**, *51*, 10558–10570. https://doi.org/10.1039/d2dt01706g.
(50) Arnold, J.; Wilkinson, G.; Hussain, B.; Hursthouse, M. B. Redox Chemistry of the Homoleptic Aryl Os(2-$MeC_6H_4)_4$: Synthesis and Characterization of the First Osmium(v) Organometallic [Os(2-$MeC_6H_4)_4$][CF_3SO_3]. *J Chem Soc Chem Commun* **1988**, *20*, 1349–1350.
(51) Gray, H. B. Molecular Orbital Theory for Transition Metal Complexes. *J. Chem. Educ.* **1964**, *41* (1), 2. https://doi.org/10.1021/ed041p2.
(52) Tanaka, Y.; Kiguchi, M.; Akita, M. Inorganic and Organometallic Molecular Wires for Single-Molecule Devices. *Chem. - Eur. J.* **2017**, *23* (20), 4741–4749. https://doi.org/10.1002/chem.201604812.
(53) Vezzoli, A. Metal Complexes and Clusters in Single-Molecule Electronics. In *Encyclopedia of Inorganic and Bioinorganic Chemistry*; Scott, R. A., Ed.; Wiley, 2021; pp 1–21. https://doi.org/10.1002/9781119951438.eibc2787.
(54) Deng, J.-R.; González, M. T.; Zhu, H.; Anderson, H. L.; Leary, E. Ballistic Conductance through Porphyrin Nanoribbons. *J. Am. Chem. Soc.* **2024**, *146* (6), 3651–3659. https://doi.org/10.1021/jacs.3c07734.
(55) Leary, E.; Limburg, B.; Alanazy, A.; Sangtarash, S.; Grace, I.; Swada, K.; Esdaile, L. J.; Noori, M.; González, M. T.; Rubio-Bollinger, G.; Sadeghi, H.; Hodgson, A.; Agraït, N.; Higgins, S. J.; Lambert, C. J.; Anderson, H. L.; Nichols, R. J. Bias-Driven Conductance Increase with Length in Porphyrin Tapes. *J. Am. Chem. Soc.* **2018**, *140* (40), 12877–12883. https://doi.org/10.1021/jacs.8b06338.
(56) Lovat, G.; Choi, B.; Paley, D. W.; Steigerwald, M. L.; Venkataraman, L.; Roy, X. Room-Temperature Current Blockade in Atomically Defined Single-Cluster Junctions. *Nat. Nanotechnol.* **2017**, *12*, 1050–1054.
(57) Kim, B.; Beebe, J. M.; Olivier, C.; Rigaut, S.; Touchard, D.; Kushmerick, J. G.; Zhu, X.-Y.; Frisbie, C. D. Temperature and Length Dependence of Charge Transport in Redox-Active Molecular Wires Incorporating Ruthenium(II) Bis(Sigma-Arylacetylide) Complexes. *J Phys Chem C* **2007**, *111* (20), 7521–7526.
(58) Lee, W.; Li, L.; Camarasa-Gómez, M.; Hernangómez-Pérez, D.; Roy, X.; Evers, F.; Inkpen, M. S.; Venkataraman, L. Photooxidation Driven Formation of Fe-Au Linked Ferrocene-Based Single-Molecule Junctions. *Nat. Commun.* **2024**, *15* (1), 1439. https://doi.org/10.1038/s41467-024-45707-z.
(59) Skipper, H. E.; May, C. V.; Rheingold, A. L.; Doerrer, L. H.; Kamenetska, M. Hard–Soft Chemistry Design Principles for Predictive Assembly of Single Molecule-Metal Junctions. *J. Am. Chem. Soc.* **2021**, *143* (40), 16439–16447. https://doi.org/10.1021/jacs.1c05142.
(60) Olivar, C.; Parr, J. M.; Avedian, C.; Saal, T.; Zagami, L.; Haiges, R.; Sharma, M.; Inkpen, M. S. Osmium(IV) Tetraaryl Complexes Formed from Pre-Functionalized Ligands. *ChemRxiv* **2024**, DOI: 10.26434/chemrxiv-2024-2ksw1.
(61) Yang, J.; He, W.; Denman, K.; Jiang, Y. B.; Qin, Y. A Molecular Breakwater-like Tetrapod for Organic Solar Cells. *J. Mater. Chem. A* **2015**, *3* (5), 2108–2119. https://doi.org/10.1039/c4ta05405a.

(62) Doud, E. A.; Inkpen, M. S.; Lovat, G.; Montes, E.; Paley, D. W.; Steigerwald, M. L.; Vázquez, H.; Venkataraman, L.; Roy, X. In Situ Formation of N-Heterocyclic Carbene-Bound Single-Molecule Junctions. *J. Am. Chem. Soc.* **2018**, *140* (28), 8944–8949. https://doi.org/10.1021/jacs.8b05184.
(63) Arnold, J.; Wilkinson, G.; Hussain, B.; Hursthouse, M. B. Synthesis and X-Ray Crystal Structure of Tetra(2-Methylphenyl)Molybdenum(IV), $Mo(2\text{-}MeC_6H_4)_4$. Redox Chemistry of $M(2\text{-}MeC_6H_4)_4$ Compounds of Molybdenum, Rhenium, Ruthenium, and Osmium. *Dalton Trans* **1989**, *11*, 2149. https://doi.org/10.1039/dt9890002149.
(64) Lau, M.-K.; Chim, J. L.; Wong, W.-T.; Williams, I. D.; Leung, W.-H. Synthesis and Molecular Structures of Monooxo Aryl Complexes of Osmium(VI). *Can. J. Chem.* **2001**, *79* (5–6), 607–612. https://doi.org/10.1139/v00-192.
(65) Hardy, D. T.; Wilkinson, G.; Young, G. B. Mechanistic Studies of Ligand-Induced Thermolytic Reductive Elimination of Biaryl from Tetraarylosmium(IV). *Polyhedron* **1996**, *15* (8), 1363–1373. https://doi.org/10.1016/0277-5387(95)00364-9.
(66) Venkataraman, L.; Klare, J. E.; Tam, I. W.; Nuckolls, C.; Hybertsen, M. S.; Steigerwald, M. L. Single-Molecule Circuits with Well-Defined Molecular Conductance. *Nano Lett* **2006**, *6* (3), 458–462. https://doi.org/10.1021/nl052373+.
(67) Miao, Z.; Quainoo, T.; Czyszczon-Burton, T. M.; Rotthowe, N.; Parr, J. M.; Liu, Z.; Inkpen, M. S. Charge Transport across Dynamic Covalent Chemical Bridges. *Nano Lett* **2022**, *22* (20), 8331–8338. https://doi.org/10.1021/acs.nanolett.2c03288.
(68) Yanson, A. I.; Rubio Bollinger, G.; Van Den Brom, H. E.; Agraït, N.; Van Ruitenbeek, J. M. Formation and Manipulation of a Metallic Wire of Single Gold Atoms. *Nature* **1998**, *395* (6704), 783–785. https://doi.org/10.1038/27405.
(69) Quek, S. Y.; Kamenetska, M.; Steigerwald, M. L.; Choi, H. J.; Louie, S. G.; Hybertsen, M. S.; Neaton, J. B.; Venkataraman, L. Mechanically Controlled Binary Conductance Switching of a Single-Molecule Junction. *Nat. Nanotechnol.* **2009**, *4* (4), 230–234. https://doi.org/10.1038/nnano.2009.10.
(70) Klausen, R. S.; Widawsky, J. R.; Steigerwald, M. L.; Venkataraman, L.; Nuckolls, C. Conductive Molecular Silicon. *J. Am. Chem. Soc.* **2012**, *134* (10), 4541–4544. https://doi.org/10.1021/ja211677q.
(71) Quek, S. Y.; Choi, H. J.; Louie, S. G.; Neaton, J. B. Length Dependence of Conductance in Aromatic Single-Molecule Junctions. *Nano Lett.* **2009**, *9* (11), 3949–3953. https://doi.org/10.1021/nl9021336.
(72) Olah, G. A. Stable Carbonium Ions in Solution. *Sci. New Ser.* **1970**, *168* (3937), 1298–1311.
(73) Kim, K.-C.; Reed, C. A.; Elliott, D. W.; Mueller, L. J.; Tham, F.; Lin, L.; Lambert, J. B. Crystallographic Evidence for a Free Silylium Ion. *Science* **2002**, *297* (5582), 825–827. https://doi.org/10.1126/science.1073540.
(74) Prana, J.; Kim, L.; Czyszczon-Burton, T.; Homann, G.; Chen, S.; Miao, Z.; Camarasa-Gomez, M.; Inkpen, M. Lewis-Acid Mediated Reactivity in Single-Molecule Junctions. *J Am Chem Soc* **2024**, *146* (48), 33265–33275. https://doi.org/10.1021/jacs.4c14176.
(75) Ghasemi, S.; Ornago, L.; Liasi, Z.; Johansen, M. B.; Von Buchwald, T. J.; Hillers-Bendtsen, A. E.; Van Der Poel, S.; Hölzel, H.; Wang, Z.; Amombo Noa, F. M.; Öhrström, L.; Mikkelsen, K. V.; Van Der Zant, H. S. J.; Lara-Avila, S.; Moth-Poulsen, K. Exploring the Impact of Select Anchor Groups for Norbornadiene/Quadricyclane Single-Molecule Switches. *J. Mater. Chem. C* **2023**, *11* (44), 15412–15418. https://doi.org/10.1039/D3TC02652C.

(76) Kawai, S. Discussion on Decomposition of Chloroform. *YAKUGAKU ZASSHI* **1966**, *86* (12), 1125–1132. https://doi.org/10.1248/yakushi1947.86.12_1125.
(77) Traverso, O.; Scandola, F. Photooxidation of Ferrocene in Halocarbon Solvents. *Inorganica Chim. Acta* **1970**, *4*, 493–498. https://doi.org/10.1016/S0020-1693(00)93335-8.
(78) Fatemi, V.; Kamenetska, M.; Neaton, J. B.; Venkataraman, L. Environmental Control of Single-Molecule Junction Transport. *Nano Lett.* **2011**, *11* (5), 1988–1992. https://doi.org/10.1021/nl200324e.
(79) Nagahara, L. A.; Thundat, T.; Lindsay, S. M. Preparation and Characterization of STM Tips for Electrochemical Studies. *Rev. Sci. Instrum.* **1989**, *60* (10), 3128–3130. https://doi.org/10.1063/1.1140590.
(80) Capozzi, B.; Low, J. Z.; Xia, J.; Liu, Z.-F.; Neaton, J. B.; Campos, L. M.; Venkataraman, L. Mapping the Transmission Functions of Single-Molecule Junctions. *Nano Lett.* **2016**, *16* (6), 3949–3954. https://doi.org/10.1021/acs.nanolett.6b01592.
(81) Low, J. Z.; Capozzi, B.; Cui, J.; Wei, S.; Venkataraman, L.; Campos, L. M. Tuning the Polarity of Charge Carriers Using Electron Deficient Thiophenes. *Chem. Sci.* **2017**, *8* (4), 3254–3259. https://doi.org/10.1039/c6sc05283e.
(82) Capozzi, B.; Xia, J.; Adak, O.; Dell, E. J.; Liu, Z.-F.; Taylor, J. C.; Neaton, J. B.; Campos, L. M.; Venkataraman, L. Single-Molecule Diodes with High Rectification Ratios through Environmental Control. *Nat. Nanotechnol.* **2015**, *10* (6), 522–527. https://doi.org/10.1038/nnano.2015.97.
(83) Blum, V.; Gehrke, R.; Hanke, F.; Havu, P.; Havu, V.; Ren, X.; Reuter, K.; Scheffler, M. Ab Initio Molecular Simulations with Numeric Atom-Centered Orbitals. *Comput. Phys. Commun.* **2009**, *180* (11), 2175–2196. https://doi.org/10.1016/j.cpc.2009.06.022.
(84) Camarasa-Gómez, M.; Hernangómez-Pérez, D.; Evers, F. Spin–Orbit Torque in Single-Molecule Junctions from Ab Initio. *J Phys Chem Lett* **2024**, *15* (21), 5747–5753.
(85) Arnold, A.; Weigend, F.; Evers, F. Quantum Chemistry Calculations for Molecules Coupled to Reservoirs: Formalism, Implementation, and Application to Benzenedithiol. *J. Chem. Phys.* **2007**, *126* (17), 174101. https://doi.org/10.1063/1.2716664.
(86) Bagrets, A. Spin-Polarized Electron Transport Across Metal–Organic Molecules: A Density Functional Theory Approach. *J. Chem. Theory Comput.* **2013**, *9* (6), 2801–2815. https://doi.org/10.1021/ct4000263.
(87) Evers, F.; Korytár, R.; Tewari, S.; Van Ruitenbeek, J. M. Advances and Challenges in Single-Molecule Electron Transport. *Rev. Mod. Phys.* **2020**, *92* (3), 35001. https://doi.org/10.1103/RevModPhys.92.035001.
(88) Thoss, M.; Evers, F. Perspective: Theory of Quantum Transport in Molecular Junctions. *J. Chem. Phys.* **2018**, *148* (3), 30901. https://doi.org/10.1063/1.5003306.
(89) Venkataraman, L.; Park, Y. S.; Whalley, A. C.; Nuckolls, C.; Hybertsen, M. S.; Steigerwald, M. L. Electronics and Chemistry: Varying Single-Molecule Junction Conductance Using Chemical Substituents. *Nano Lett.* **2007**, *7* (2), 502–506. https://doi.org/10.1021/nl062923j.
(90) Edwards, P. G.; Behling, T.; Wilkinson, G.; Motevalli, M.; Hursthouse, M. B. Oxoaryls of Rhenium-(V) and -(VI) and Osmium(VI). X-Ray Crystal Structures of Dimesityldioxorhenium(VI), Tetramesityloxorhenium(VI), and Dimesityldioxoosmium(VI). *J Chem Soc Dalton Trans* **1987**, 169–175.